Two new polyoxometalates-based metal-organic complexes for the detection of trace Cr (VI) and their capacitor performance

Qian-Qian Liu, Xiu-Li Wang,* Hong-Yan Lin, Zhi-Han Chang, Yu-Chen Zhang, Yuan Tian, Jun-Jun Lu and Le Yu

College of Chemistry and Materials Engineering, Professional Technology Innovation Center of Liaoning Province for Conversion Materials of Solar Cell, Bohai University, Jinzhou 121013, P. R. China

Materials and General Methods

All reagents were purchased commercially and used without further purification. The ligand 4-H_2dpye was prepared according to a literature method.[1] Crystallographic data for complexes **1-2** were collected on a Bruker SMART APEX II with Mo Kα (λ =0.71073 Å) by ω and θ scan mode. Powder X-ray diffraction (PXRD) patterns were performed using an Ultima IV with D/teX Ultra diffractometer at 40 kV, 40 mA with Cu Kα radiation. The elemental analyses (C, H and N) were carried out on a Perkin Elmer 240C elemental analyzer. The FT-IR spectra were performed on a Varian 640-IR spectrometer (KBr pellets). The thermal stabilities of the complexes **1-2** were analyzed with a thermogravimetric analyzer (NETZSCH STA 449C). X-ray photoelectron spectroscopy (XPS) analyses were carried out with a Thermo SCIENTIFIC ESCALAB 250.

X-Ray crystallographic study

Using Olex2, the structures were solved with the SHELXT structure solution program using Intrinsic Phasing and refined with the SHELXL refinement package using Least Squares minimisation.[2] Complex **1** exhibited very large solvent accessible voids in the final refinement and the remanent peaks were too weak to be confirmed as solvent molecules. Thus, the SQUEEZE program was used to further estimate the possible solvent accessible voids and the number of solvent water molecules in the

Corresponding author. Tel.: +86-416-3400160

*E-mail addres*s: wangxiuli@bhu.edu.cn (X. L. Wang)

crystal structure. The command "DFIX" was used to refine atoms H1Wa-H3Wa in complex **2**. Additionally, further details of the crystallographic data and structures for complexes **1-2** are listed in Table S1. Selected bond lengths and angles of two complexes are listed in Table S2. Crystallographic data for the structures reported in this paper have been deposited in the Cambridge Crystallographic Data Center with CCDC number 2043829 and 2043695.

XPS, PXRD, IR and TGA analysis

The high-resolution Mo3d peaks at 232.8 and 232.7 eV in complex **1** and complex **2** correspond to $Mo^{VI}3d_{5/2}$, and the peaks at 235.9 and 235.8 eV correspond to $Mo^{VI}3d_{3/2}$. The results show that all Mo atoms in complexes **1** and **2** are in +VI oxidation state[3], as shown in Fig. S1a-b

The powder X-ray diffraction (PXRD) of **1** and **2** as well as their simulated PXRD patterns are shown in Fig. S2a-b. The diffraction peaks on the patterns correspond well in position, confirming that the products are in a pure phase. The differences in reflection intensity are probably due to the different orientation in the powder samples.[4]

The IR spectra of complexes **1-2** are shown in Fig. S3a-b. For complexes **1-2**, characteristic bands at 1250-1650 cm^{-1} can be attributed to the characteristic peaks of C=O and N-H in the 4-H_2dpye ligand. The wider band around 3500 cm^{-1} can be attributed to water molecules. The characteristic bands at 959, 878, 800, 1060 cm^{-1} for complex **1**, 948 876 803 1052 cm^{-1} for complex **2** can be attributed to ν_{as} (Mo-O_t), ν_{as} (Mo-O_b-Mo), ν_{as} (Mo-O_c-Mo) and ν (P-O) of PMo_{12} polyoxoanions, respectively.[5]

Thermogravimetric analyses (TGA) of complexes **1-2** are performed to study their thermal behaviors. In the temperature range of 25−800 °C, complex **1** shows only a weight loss process, which can be attributed to the decomposition of the ligands. The TG curve of complex **2** shows a two-step weight loss process. The first below 250 °C can be ascribed to loss of the coordinated and lattice water molecules. Upon further heating, the framework of complex **2** began to collapse after 250 °C, indicating the decomposition of organic ligands, as shown in Fig. S4 a-b.

Preparation of working electrode

The complex **1** bulk-modified carbon paste electrode (**1**-CPE) was fabricated as follows: 0.01 g of complex **1** and 0.1 g of graphite powder were mixed and grind vigorously for 30 minutes in an agate mortar to form a uniform mixture. Then 0.1 mL of liquid paraffin was added with stirring. The homogenized mixture was packed into a glass tube with a 2.4 mm inner diameter, and the tube surface was wiped with weighing paper. Electrical contact was established with a copper rod through the back of the electrode. In a similar manner, **2**-CPE was made with complex **2**.

0.5 × 2 cm^2 carbon cloth (CC) was cut out and treated with HNO_3, H_2O, and ethanol in sequence. Then vacuum dry was performed at 80 °C for 10 h. The electrode material based on complex **1** (**1**-CC) was prepared as following: Ketjen black (KB) (0.002 g), complex **1** (0.002 g) and Poly (vinylidene fluoride) (PVDF) (0.001 g) were ground together in an agate mortar for 1 hour to obtain a mixture; 0.10 mL N-Methy pyrrolidone (NMP) was added and stirred to get a black paste; The paste was coated onto one side of the treated CC; Finally, vacuum drying at 80 °C for 12 h. The preparation method of **2**-CC was similar to that of **1**-CC.

Electrochemical measurements

A CHI760 electrochemical workstation was used for control of the electrochemical measurements and data collection. **1**-CPE and **2**-CPE were used as working electrodes, commercial Ag/AgCl was used as a reference electrode, and twisted platinum wire was used as a counter electrode (in 0.1 M H_2SO_4 + 0.5 M Na_2SO_4) to study the electrocatalytic performances of **1**-CPE and **2**-CPE.

The following formula was used to calculate the lower limit of detection (LOD) of **1**-CPE and **2**-CPE to Cr (VI):

$$LOD = \frac{S/N \cdot \sigma}{k}$$

Among them, S/N is the signal-to-noise ratio, and usually the value is 3, σ is the standard deviation of the y-intercept of the regression line, and k is the linear regression slope.[6]

Moreover, galvanostatic charge/discharge and electrochemical impedance spectroscopy (EIS) measurements were based on **1**-CC and **2**-CC as working

electrodes, the saturated calomel electrode (in 0.1 M H_2SO_4) was used as reference electrode and the graphite rod was used as counter electrode.

The specific gravimetric capacitance value can be calculated from the following equation:

$$C_s = \frac{I\Delta t}{m\Delta V}$$

where Cs (F g^{-1}) represents the specific capacitance, I (A) represents the discharge current, ΔV (V) represents the potential change within the discharge time Δt (s), and m (g) corresponds to the amount of active material on the electrode.[7]

Table S1. Crystallographic data for complexes **1-2**.

Complex	**1**	**2**
Empirical formula	$C_{24}H_{23}Cu_2Mo_{12}N_{12}O_{44}P$	$C_{24}H_{33}Cu_2Mo_{12}N_{12}O_{50}P$
Formula weight	2489.85	2599.96
Crystal system	Monoclinic	Triclinic
Space group	C2/m	P -1
a (Å)	15.5819(7)	11.6974(14)
b (Å)	16.9947(7)	11.8807(13)
c (Å)	13.2208(6)	12.1832(14)
α (°)	90	67.854(2)
β (°)	119.4080(10)	74.137(2)
γ (°)	90	75.682(2)
V (Å ^{3})	3049.9(2)	1488.6(3)
Z	2	1
D_c (g cm^{-3})	2.711	2.900
μ (mm^{-1})	3.195	3.287
F (000)	2354	1239
Reflection collected	12902	10628
Data/restraints/parameters	4980/0/255	6966/2/479
Goodness-of-fit on F^2	1.039	1.049
Final R indexes [I>=2σ (I)]	R_1 = 0.0433, wR_2 = 0.0980	R_1 = 0.0507, wR_2 = 0.0941
Final R indexes [all data]	R_1 = 0.0672, wR_2 = 0.1103	R_1 = 0.0788, wR_2 = 0.1056

[a] $R_1 = \Sigma||F_o|-|F_c||/\Sigma|F_o|$, [b] $wR_2 = \Sigma[w(F_o^2-F_c^2)^2]/\Sigma[w(F_o^2)^2]^{1/2}$

Table S2. Selected bond distances (Å) and angles (°) for complexes **1-2.**

Complex **1**			
Cu(1)-O(1)	1.945(5)	O(1)#4-Cu(1)-N(1)	82.9(2)
Cu(1)-O(1)#4	1.945(5)	O(1)#4-Cu(1)-N(1)#4	82.9(2)
Cu(1)-O(2)	2.545(4)	O(1)-Cu(1)-N(1)#4	97.1(2)
Cu(1)-O(2)#4	2.545(4)	O(1)#4-Cu(1)-N(1)	97.1(2)
Cu(1)-N(1)	1.945(4)	N(1)-Cu(1)-O(2)	91.32(14)
Cu(1)-N(1)#4	1.944(4)	N(1)#4-Cu(1)-O(2)	88.68(14)
O(1)-Cu(1)-O(2)	90.96(17)	N(1)-Cu(1)-N(1)#4	180.0
O(1)#4-Cu(1)-O(2)	89.04(17)	O(1)#4-Cu(1)-N(1)#4	97.1(2)
O(1)-Cu(1)-O(1)#4	180.0	C(2)-N(1)-Cu(1)	113.8(4)
O(1)-Cu(1)-N(1)	82.9(2)	C(4)-N(1)-Cu(1)	127.2(5)
Symmetry code: #4 -x+3/2,-y+3/2,-z+2;			
Complex **2**			
Cu(1)-O(1)	2.026(5)	O(1)-Cu(1)-O(2)#2	83.0(3)
Cu(1)-N(1)	1.999(6)	O(1)-Cu(1)-O(2W)	82.1(3)
Cu(1)-O(2)#2	2.319(6)	N(1)-Cu(1)-O(1)	80.6(2)
Cu(1)-N(2)#2	2.011(6)	N(1)-Cu(1)-O(2)#2	99.1(2)
Cu(1)-O(1W)	1.953(6)	N(1)-Cu(1)-N(2)#2	171.8(2)
Cu(1)-O(2W)	2.263(8)	N(1)-Cu(1)-O(2W)	92.0(3)
O(1W)-Cu(1)-O(1)	171.3(3)	N(2)#2-Cu(1)-O(1)	92.4(2)
O(1W)-Cu(1)-N(1)	94.4(2)	N(2)#2-Cu(1)-O(2)#2	75.8(2)
O(1W)-Cu(1)-O(2)#2	104.8(3)	N(2)#2-Cu(1)-O(2W)	91.1(3)
O(1W)-Cu(1)-N(2)#2	93.2(3)	O(2W)-Cu(1)-O(2)#2	159.7(3)
O(1W)-Cu(1)-O(2W)	91.1(3)		
Symmetry code: #2 -x+1,-y,-z+1			

Table S3. Selected hydrogen-bonding geometry (Å, °) for complex **2.**

D-H···A	D-H	H···A	D···A	D-H···A

N(5)-H(5)···O(3)	0.86	2.02	2.852(9)	164
O(2W)-H(2WB)···N(4)	0.88	2.40	2.767(13)	106
O(1W)-H(1WA)···O(19)	0.93	2.57	3.002(10)	109

Table S4. Summary of the typical crystal POMs-based MOCs supercapacitor electrode materials

Electrode	Cs (F g^{-1})	Current density (A g^{-1})	Ref.
1-CC	**260.0**	**0.5**	**This work**
2-CC	**196.6**	**0.5**	**This work**
$[H(C_{10}H_{10}N_2)Cu_2][PMo_{12}O_{40}]$	287	1	8
$[H(C_{10}H_{10}N_2)Cu_2][PW_{12}O_{40}]$	153.4	1	8
$[Cu^{I}_4H_2(btx)_5(PW_{12}O_{40})_2]\cdot 2H_2O$	100	2	9
$[Cu^{II}Cu^{I}_3(btx)_5(SiMo^{VI}_{11}Mo^{V}O_{40})]\cdot 4H_2O$	138	2	9
$(H_2bipy)_{1.5}[Cu^{I}(bipy)(C_6H_5PO_3)_2Mo_5O_{15}]\cdot H_2O$	70.3	2	10
$[Cu^{II}_2(bipy)(H_2O)_4(C_6H_5PO_3)_2Mo_5O_{15}]$	160.9	2	10
$H_3PMo^{VI}_{12}O_{40}\cdot(BPE)_{2.5}\cdot 3H_2O$	137.5	2	11
$[Ag_5(C_2H_2N_3)_6][H_5 \subset SiMo_{12}O_{40}]$	155	0.5	11
$[Ag_5(C_2H_2N_3)_6][H_5 \subset SiMo_{12}O_{40}]$@15%GO	230.2	0.5	12
$[Ag_{10}(C_2H_2N_3)_6][SiW_{12}O_{40}]$	47.8	1.5	13
$[Ag(C_2H_2N_3)][Ag_{12}(C_2H_2N_3)_9][H_2BW_{12}O_{40}]$	42.9	1.5	13

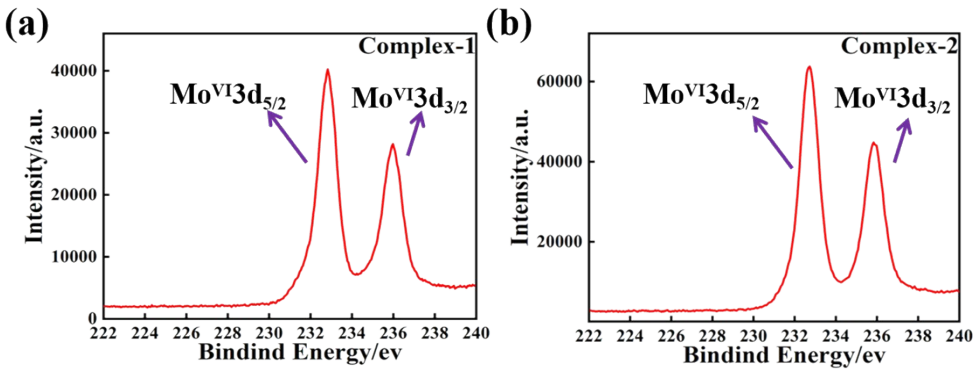

Fig. S1 (a-b) The XPS spectra for Mo(3d) in complexes **1-2**.

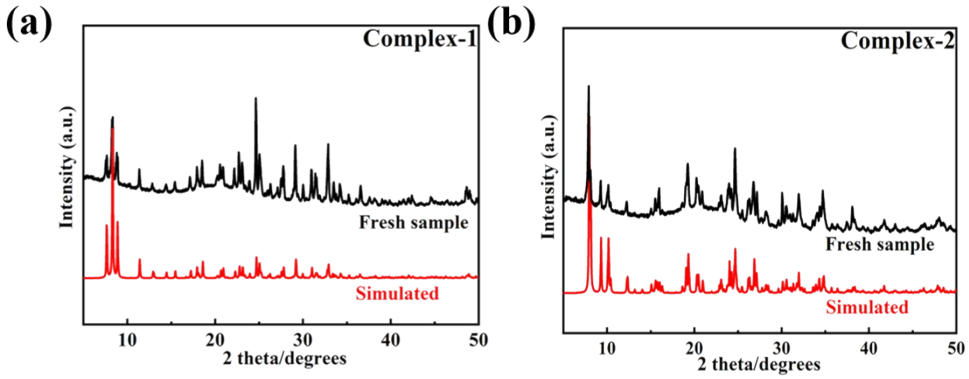

Fig. S2 (a-b) Powder X-ray diffraction patterns of complexes **1**-**2**

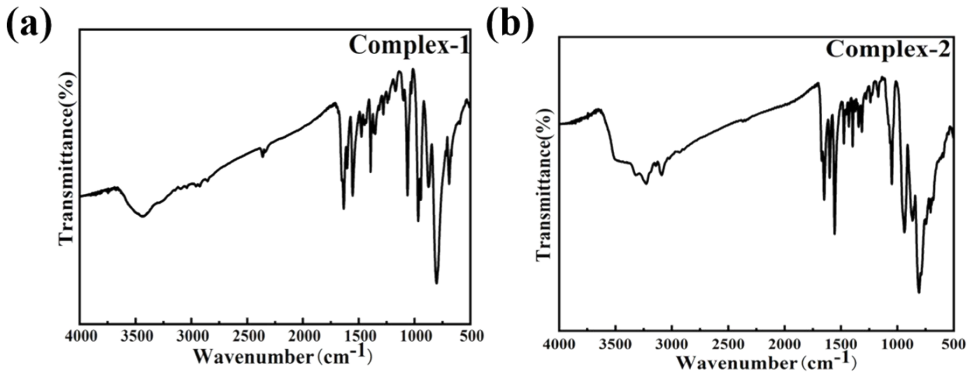

Fig. S3 (a-b) The IR spectra of complexes **1**-**2**

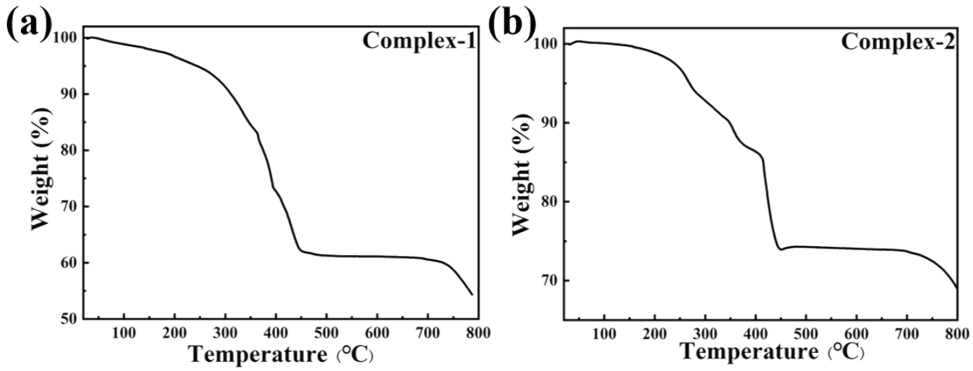

Fig. S4 (a-b) The TGA curves of complexes **1**-**2**.

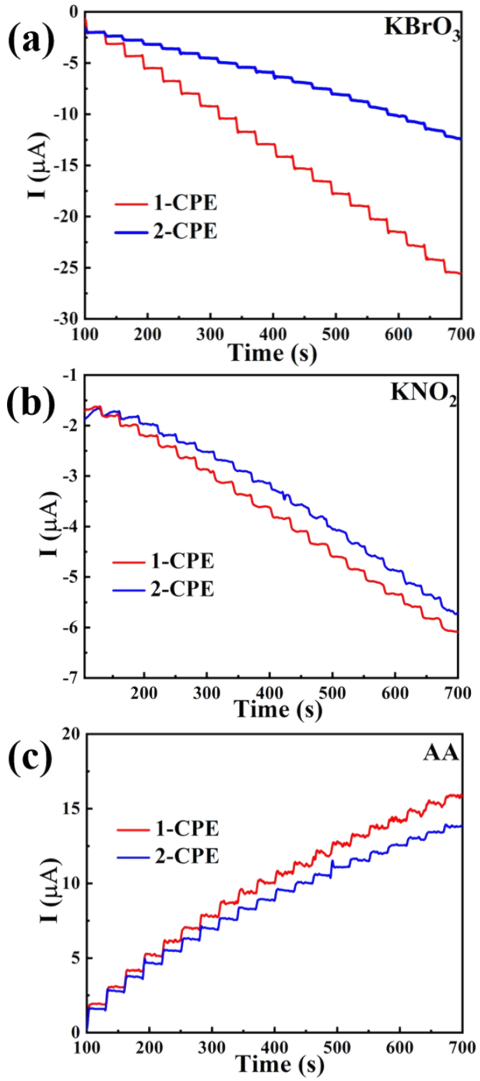

Fig. S5 Amperometric response for the **1**-CPE and **2**-CPE on successive addition of 0.1 mM BrO_3^- (a); NO_2^- (b) and AA (c) to 0.1 M H_2SO_4 + 0.5 M Na_2SO_4 aqueous solution, respectively.

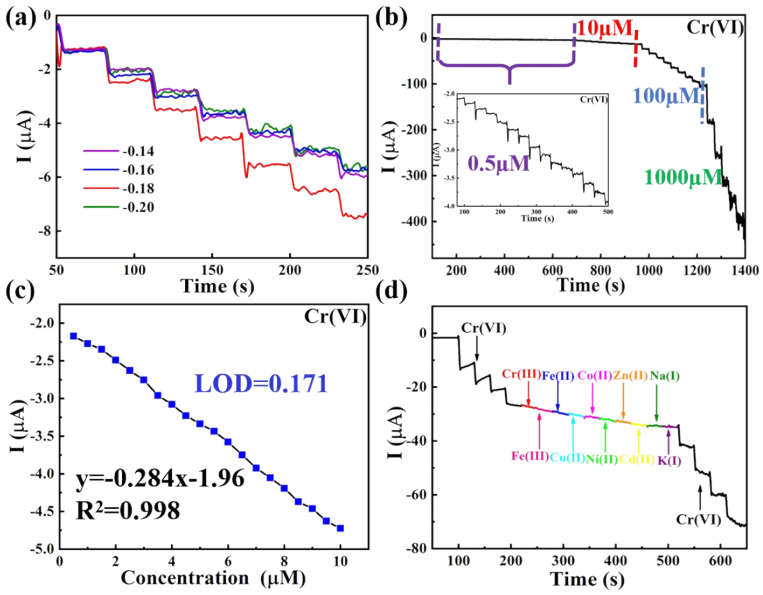

Fig. S6 (a) Ampere current response of **2**-CPE at different potentials (-0.2 V, -0.18 V, -0.16 V and -0.14 V); (b) Amperometric response of **2**-CPE continuously adding different concentrations of Cr(VI); (c) The calibration curves between the currents and concentrations of Cr(VI) measured by **2**-CPE; (d) Amperometric current responses of **2**-CPE changing with the successive additions of metal ions (250 μM of Cr^{3+}, Fe^{3+}, Fe^{2+}, Cu^{2+}, Co^{2+}, Ni^{2+}, Zn^{2+}, Cd^{2+}, Na^{+}, K^{+}) in 0.1 M H_2SO_4 + 0.5 M Na_2SO_4 solution.

References

1. X. L. Wang, J. Luan, H. Y. Lin, M. Le and G. C. Liu, *Dalton Trans.*, 2014, **43**, 8072-8082.

2. O. V. Dolomanov, L. J. Bourhis, R. J. Gildea, J. A. Howard and H. Puschmann, *J Appl Crystallogr*, 2009, **42**, 339-341.

3 X. Yang, J. Sha, W. Li, Z. Tan, L. Hou and J. Jiang, *ACS Sustainable Chem. Eng*, 2020, **8**, 4667-4675.

4. P. P. Zhang, J. Peng, J. Q. Sha, A. X. Tian, H. J. Pang, Y. Chen and M. Zhu, *CrystEngComm*, 2009, **11**, 902-908.

5 C. R. Deltcheff, M. Fournier, R. Franck and R. Thouvenot, *Inorg. Chem.*, 1983, **22**, 207-216.

6 R. Liu, Y. Luo, Y. Zheng, G. Zhang and C. Streb, *Chem. Commun.*, 2020, **56**, 9465-9468.

7. Y. Hou, D. Chai, B. Li, H. Pang, H. Ma, X. Wang and L. Tan, *ACS Appl. Mater. Interfaces*, 2019, **11**, 20845-20853.

8 S. Roy, V. Vemuri, S. Maiti, K. S. Manoj, U. Subbarao and S. C. Peter, *Inorg. Chem.*, 2018, **57**,

12078-12092.

9 D. Chai, C. J. Gomez-Garcia, B. Li, H. Pang, H. Ma, X. Wang and L. Tan, *Chem. Eng. J.* , 2019, **373**, 587-597.

10 B. Lu, S. Li, J. Pan, L. Zhang, J. Xin, Y. Chen and X. Tan, *Inorg. Chem.*, 2020, **59**, 1702-1714.

11 C. Wang, S. Rong, Y. Zhao, X. Wang and H. Ma, *Transition Met. Chem.*, 2021, **46**, 335-343

12 Y. Hou, D. Chai, B. Li, H. Pang, H. Ma, X. Wang and L. Tan, *ACS Appl. Mater. Interfaces*, 2019, **11**, 20845-20853.

13 Y. Hou, H. Pang, C. J. Gomez-Garcia, H. Ma, X. Wang and L. Tan, *Inorg. Chem.*, 2019, **58**, 16028-16039.